Chapter 4 The formation mechanisms of Cr(VI)-containing electric furnace dust and filter cake from a stainless steel waste treatment plant

In order to minimise the generation of these wastes, the microstructures and formation mechanisms of the wastes first need to be understood. This chapter subsequently describes the microstructures and formation mechanisms of the dust and filter cake in order to provide suggestions on how to reduce the amounts of these wastes.

4.1 Experimental

4.1.1 Sample Preparation

Three ferrochrome dusts samples (FCD1, FCD2 and FCD3), one stainless steel plant dust sample (SPD) and a filter cake sample (FC) were obtained from the same ferrochromium and stainless steel plants as discussed in Chapter 3. Representative sub-samples were produced from each of these samples for analysis.

4.1.2 Analytical Methods

Polished sections of the electric furnace dust and filter cake as well as the unmounted samples of waste were examined by scanning electron microscopy (JSM-6300), using energy dispersive X-ray spectrometry (EDS). The crystalline phases present in the samples were identified by X-ray diffraction (XRD) (Siemens D-501, Cu *K*α radiation, 40kV and 40mA).

4.2 Results

4.2.1 Steel plant dust

Stainless steel plant dust particles are of varying microstructure, and can be divided into three categories: (1) particles that are irregular in shape, (2) spherical or near spherical particles and (3) particles coated with slag or oxides. The particles that are spherical or near spherical, as well as the spherical particles that are coated with slag or oxides, are the most abundant in the SPD sample.

The particles that are irregular in shape include pure nickel (Figure 4.1), quartz, lime, fluorspar and ferrochrome particles. It is clear that these particles were captured by the off-gas during charging.

The spherical or near spherical particles include metal particles (Figure 4.2) and slag particles. These particles range from submicron to more than 200µm in diameter. The slag particles are either hollow (Figure 4.3) or consist of a glassy silicate-based matrix that contains oxide crystals (Figures 4.4-4.6) and metal droplets (Figure 4.7). The oxide crystals are either cubic (Figure 4.4), dendritic (Figure 4.5) or needle-like (Figure 4.6). EDS analysis indicated that the cubic and dendritic crystals are $(Mg,Fe,Mn)(Cr,Al)_2O_4$ spinel crystals, while the needles are $CaCr_2O_4$. Spherical stainless steel particles (Fe-3.0 wt% Cr-7.2 wt% Ni-3.9wt% Mo) that are coated with slag were also found (Figure 4.7). Slag particles that are covered with an oxide layer, which is of different chemical composition to the centre of the particle, could also be distinguished. Such slag particles are shown in Figures 4.8 and 4.9. X-ray mapping indicated that the centres of these types of particle are enriched in Cr, Ca and Al, while the rim is rich in Zn and Fe (Figure 4.9).

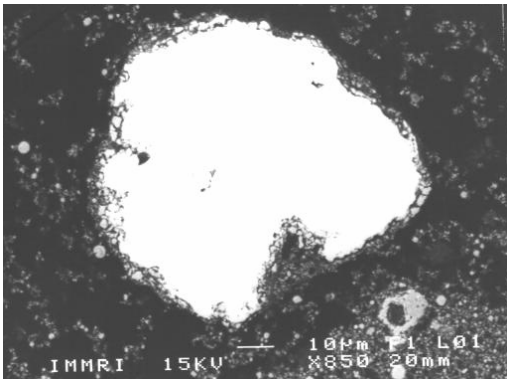

Figure 4.1 A nickel particle (SPD).

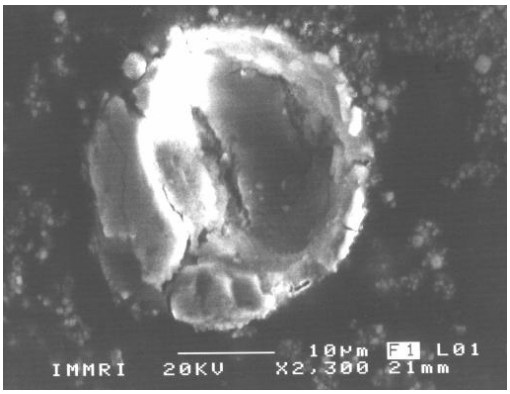

Figure 4.2 A hollow spherical metal particle (SPD).

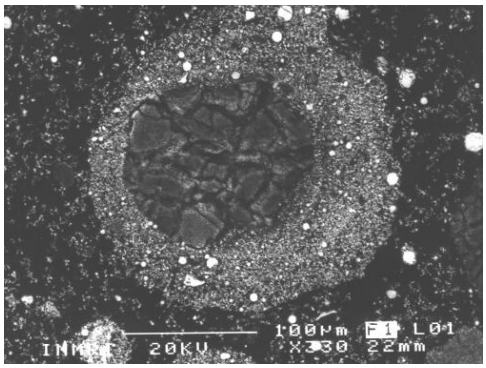

Figure 4.3 A hollow slag particle (SPD).

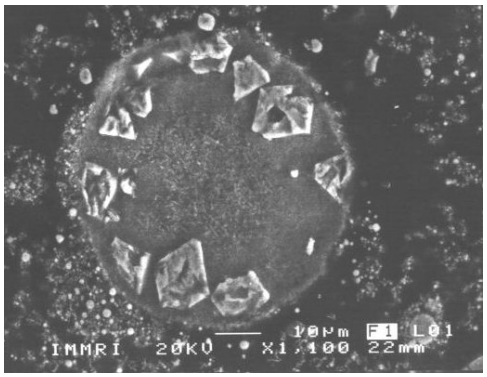

Figure 4.4 A spherical slag particle with cubic spinel crystals (SPD).

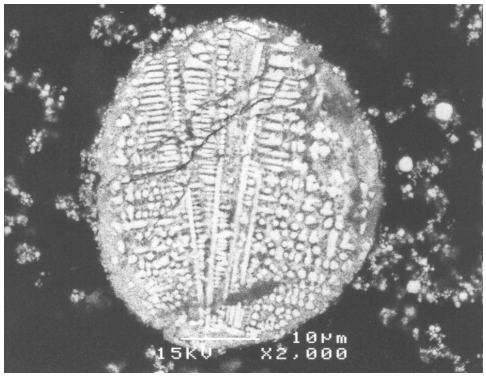

Figure 4.5 A spherical particle with dendritically precipitated crystals (SPD).

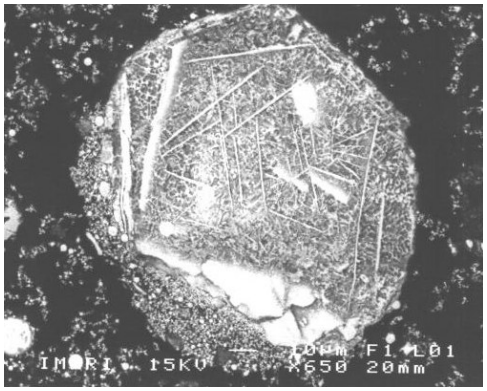

Figure 4.6 A spherical particle with precipitated $CaCr_2O_4$ needles (SPD).

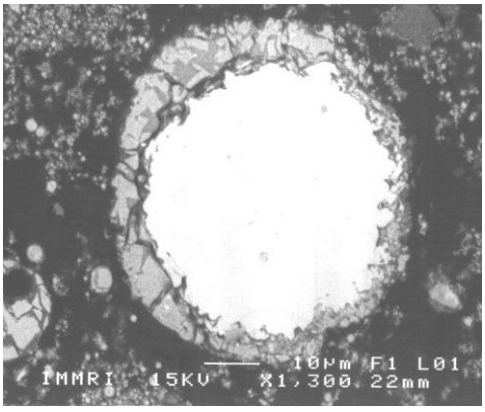

Figure 4.7 A stainless steel droplet, coated with slag (SPD).

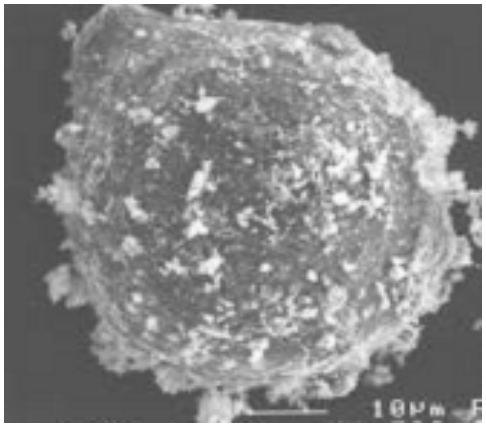

Figure 4.8 Slag droplet with a rim of small particles (SPD).

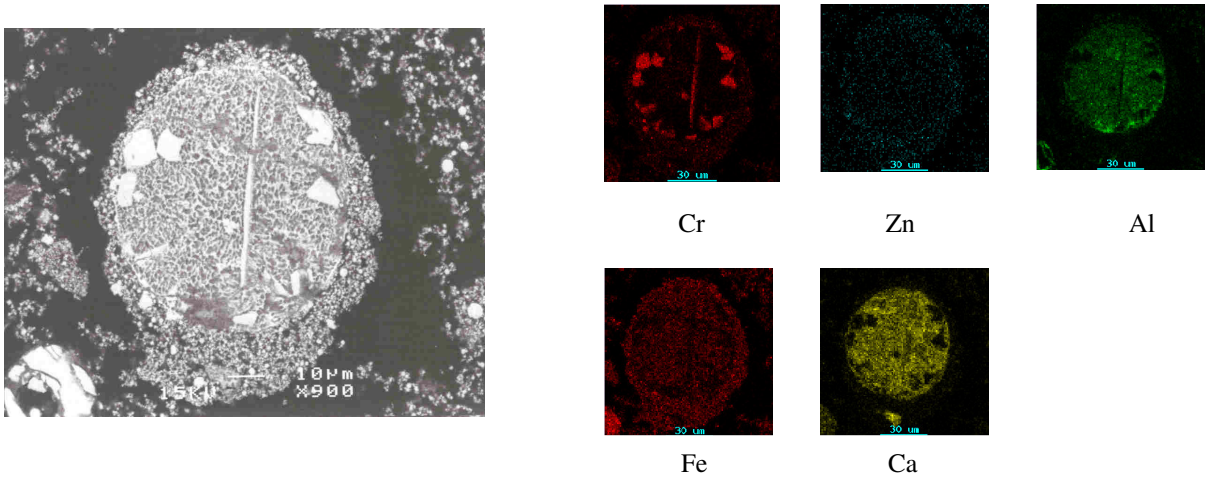

Figure 4.9 Backscattered electron image and X-ray map of a slag particle coated with a Fe-Zn-rich oxide layer (SPD)

4.2.2 Ferrochrome plant dust

The fine fractions of ferrochrome dusts (FCD1 and FCD2) mostly consist of agglomerated particles that formed clusters (Figures 4.10 and 4.11). Such clusters typically contain chromite and partly altered chromite (PAC) particles, reductant (C-based particles), metallic ferrochrome droplets, flux (quartz) and SiO_2-based slag droplets that are embedded in a matrix of very fine particles. This matrix is mainly SiO_2-MgO-ZnO-$(Na,K)_2O$ based.

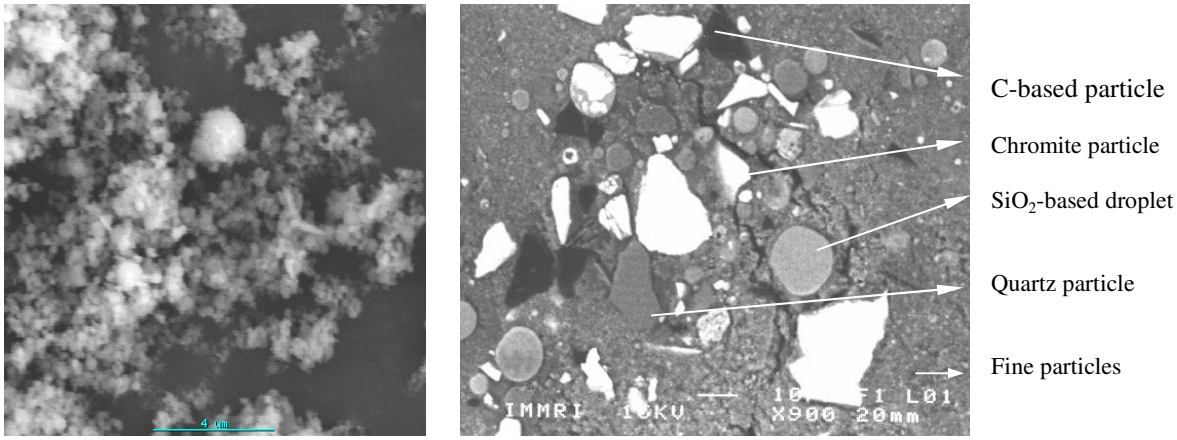

Figure 4.10 The FCD2 ferrochrome dust sample: (a) Agglomerated fine dusts; (b) Backscattered electron image of the typical microstructure.

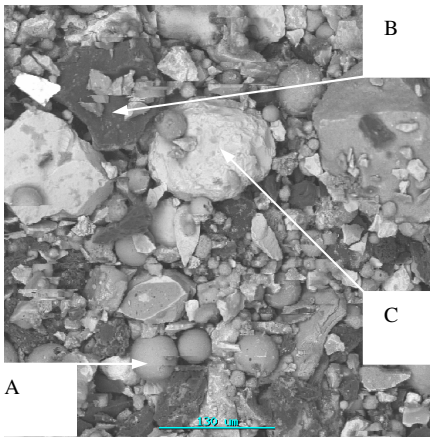

Figure 4.11 Microstructure of the FCD3 ferrochromium EF dust. (A): Slag droplet, (B) carbon-bearing material; (C) chromite ore.

The coarse fraction (FCD3) mostly contains particles that are irregular in shape, but also spherical or near spherical particles and particles coated with a slag layer. The particles that are irregular in shape include chromite ore particles, quartz particles and carbon-based particles. The spherical particles include metal particles, Si-Ca-Mg-Fe based slag particles, particles that contain spinel crystals and ferrochrome droplets that are embedded in a porous sodium-rich silicate slag layer (Figure 4.12), as well as chromite particles that are surrounded with a porous layer that contains some very small Cr-Fe-based metal droplets, followed by a more solid layer of Mg_2SiO_4 (Figure 4.13).

4.2.3 Filter Cake

The filter cake consists of very finely intergrown light grey areas that are Ca-F-S-O based, and dark areas that contain high concentrations of metal oxides of iron, chromium and nickel (Figure 4.14). XRD analysis indicated that the Ca-F-S-O-based areas consist of a mixture of CaF_2 and $CaSO_4$ while the metal-rich oxide phase is amorphous. The Ca-F-S-O based precipitate presumably formed due to super-saturation of the waste acid with respect to CaF_2 and $CaSO_4$ (solubility limits of 0.016g/l and 2.09g/l respectively [67]) in the neutralisation and reduction steps. It is assumed that the metal oxide-rich precipitate is the reaction product between the metal ions and the lime particles during the final

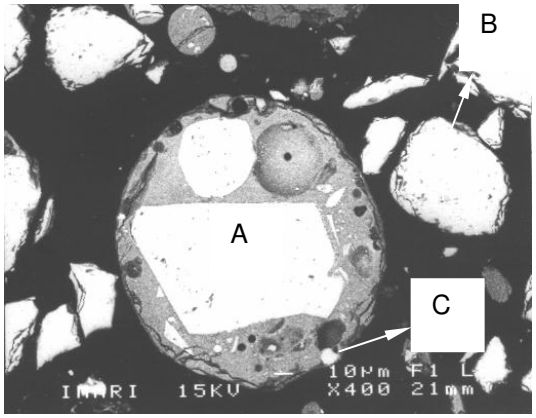

Figure 4.12 Spinel crystal in a sodium-rich silicate slag matrix (FCD3). [A=spinel crystal; B=PAC; C=FeCr droplet]

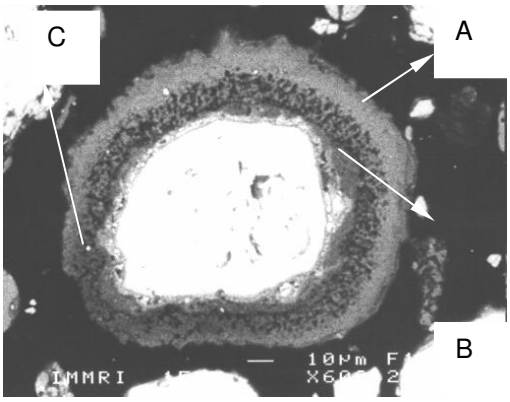

Figure 4.13 PAC particle with a Mg_2SiO_4-based rim (FCD3). [A=Mg_2SiO_4 rim; B=porous layer; C=FeCr droplets]

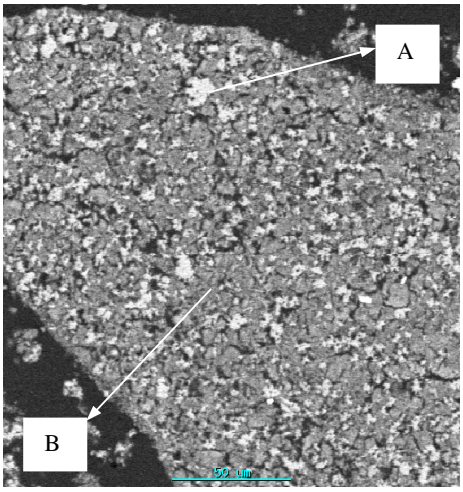

Figure 4.14 Typical SEM image of FC[A=Ca-S-F-O rich phase; B=Metal rich phase]

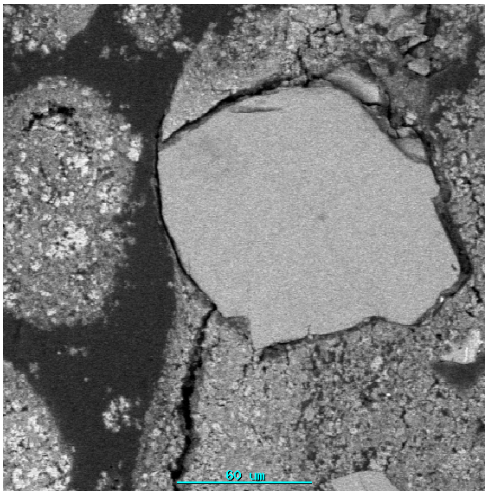

Figure 4.15 An un-reacted lime particle in the FC

precipitation step. Free lime particles (Figure 4.15) and undissolved stainless steel scale could also be distinguished in the filter cake.

4.3 Discussion

4.3.1 The formation mechanisms of stainless steel plant dust

Three different dust formation mechanisms have been reported to contribute to dust generation in the EAF and refining converter of stainless steel plants [23-37], i.e.,

(1) direct entrainment of the charged materials in the off-gas;

(2) evaporation or volatilisation of elements in the melting bath or high temperature zone of the furnace and later, oxidization or solidification of these elements in the off-gas duct and;

(3) ejection of slag and metal by spitting or bursting of gas bubbles such as carbon monoxide and argon gas. In the EAF and refining converter, the gas bubbles could entrain a thin layer of steel, enter the molten slag layer, and then burst into very fine metal droplets. When the gases escape the gas-slag interface, the film would break up on top of the bath. The falling slag can then generate waves on the surface of the molten bath whereby film droplets and jet drops can form. Moreover, the metal and slag droplets could also be ejected in the arc and oxygen-blowing zones.

In this study, the formation mechanisms of the wastes were determined from analyses of the processes and microstructures of the wastes. Fluorite (CaF_2), quartz (SiO_2) and nickel particles that were found in the examined SPD entered the bag house system through the entrainment of the charge materials in the off-gas. The $Ca(OH)_2$ formed through the hydration of lime particles which are also carried off by off-gas. These particles are all irregular in shape. Zinc is found on the surface of the dust particles (Figure 4.9). It seems that zinc is first vaporised and later condensed.

The spherical particles consist of metallic and slag particles which come from the melting bath. Spinel crystals and metallic droplets could also be found in the slag particles. These particles enter the off-gas duct by the bursting of gas bubbles. Primary spinel crystals could be found in certain of the slag particles, while in other slag particles the spinels crystallised on cooling.

4.3.2 The formation mechanisms of the ferrochrome dust

FACT Sage 5.1 was used in the theoretical prediction of the reactions that can contribute to dust formation during the production of ferrochrome in submerged arc furnaces (SAFs) (Figure 4.16) [141].

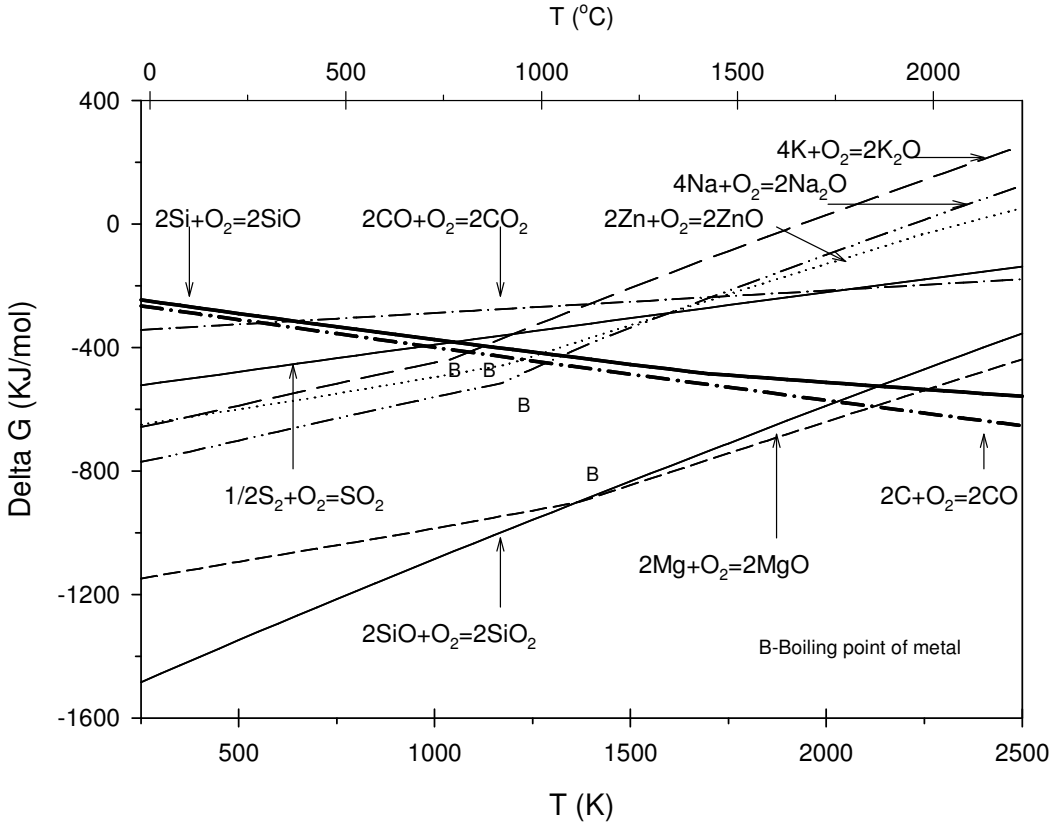

Figure 4.16 ΔG vs. temperature calculations for reactions that can contribute to dust formation during ferrochromium production, using FACT Sage 5.1

In the production of ferrochrome low oxygen partial pressures ($<10^{-8}$ atm [40]) prevail, during which the off-gas typically contains about 90% CO [8]. Under these conditions zinc, potassium and sodium in the charge can be reduced by carbon or CO gas at low temperatures (approximately 800-1100°C), after which they vaporise. These species can re-oxidise by the leakage of air or CO_2 gas and can then condense on other particles in the off-gas duct. SiO_2, which is either in the charge as quartz or in the slag, can also be reduced by carbon into SiO(g). Similarly magnesium oxide in the slag phase can be converted into Mg(g). These reactions can occur in the elevated temperature zone of the

SAF, especially near the electrode (>2000°C [142]). The SiO(g) and Mg(g) can easily re-oxidise into SiO_2 and MgO when the oxygen potential of the gas phase increases.

The moisture in the charge is also vaporised into the off-gas at high temperatures. Some inorganic components such as chlorine and sulphur from the carbon-based reductant would vaporise together with other metal elements or decompose. Coal, which contains volatile organic and inorganic substances, as well as volatile metals such as K and Na, is often used as a substitute for coke in the production of ferrochrome in order to reduce cost. The chlorine in coal typically ranges between 50-2000ppm in concentration, and vaporise at high temperatures in the form of HCl, NaCl and KCl [143,144]. Coal, coke and charcoal also contain significant levels of sulphur and heavy metals such as As, Cd and Pb. Sulphur is released into the off-gas through the formation of SO_2(g) and SO_3(g).

Gas species such as SiO, Mg, SO_2, SO_3, O_2, CO, CO_2, H_2O, Zn and NaCl, or reaction products between them, can therefore exist in the off-gas duct of the SAF. NaCl, Mg, SiO and Zn gases could first be oxidised by the off-gas and then condense. Mg_2SiO_4 can form through the reduction of chromite ore by the carbon-bearing reductant (Figure 4.13) or the reaction of SiO, Mg and oxygen in the off-gas duct. ZnO can react with SO_3 to form $ZnSO_4$ due to the oxidising atmosphere in the duct. XPS results showed that the major elements on the surface of these dusts are elements that vaporised (Chapter 3).

The synthetic hydrate samples were used to verify the possible formation of $NaZn_4(SO_4)Cl(OH)_6{\cdot}6H_2O$ and zinc sulfate hydroxide hydrate crystals in the ferrochrome fine dusts. Two mixtures were prepared from different molar ratios of ZnO, $ZnSO_4{\cdot}7H_2O$ and NaCl (AR grade), i.e. ZnO: $ZnSO_4{\cdot}7H_2O$ =3:1 and ZnO: $ZnSO_4{\cdot}7H_2O$: NaCl = 3:1:1, since ZnO, $ZnSO_4$, H_2O and NaCl possibly exist in the off-gas duct. These mixtures were placed in desiccators of which the bottoms were filled with water. The lid was closed with vacuum grease for approximately one week. The XRD patterns and SEM images of the reaction products are shown in Figure 4.17 and Figure 4.18. XRD and EDS analyse indicated that the main synthetic products are $Zn_4SO_4(OH)_6{\cdot}5H_2O$ and $NaZn_4(SO_4)Cl(OH)_6{\cdot}6H_2O$.

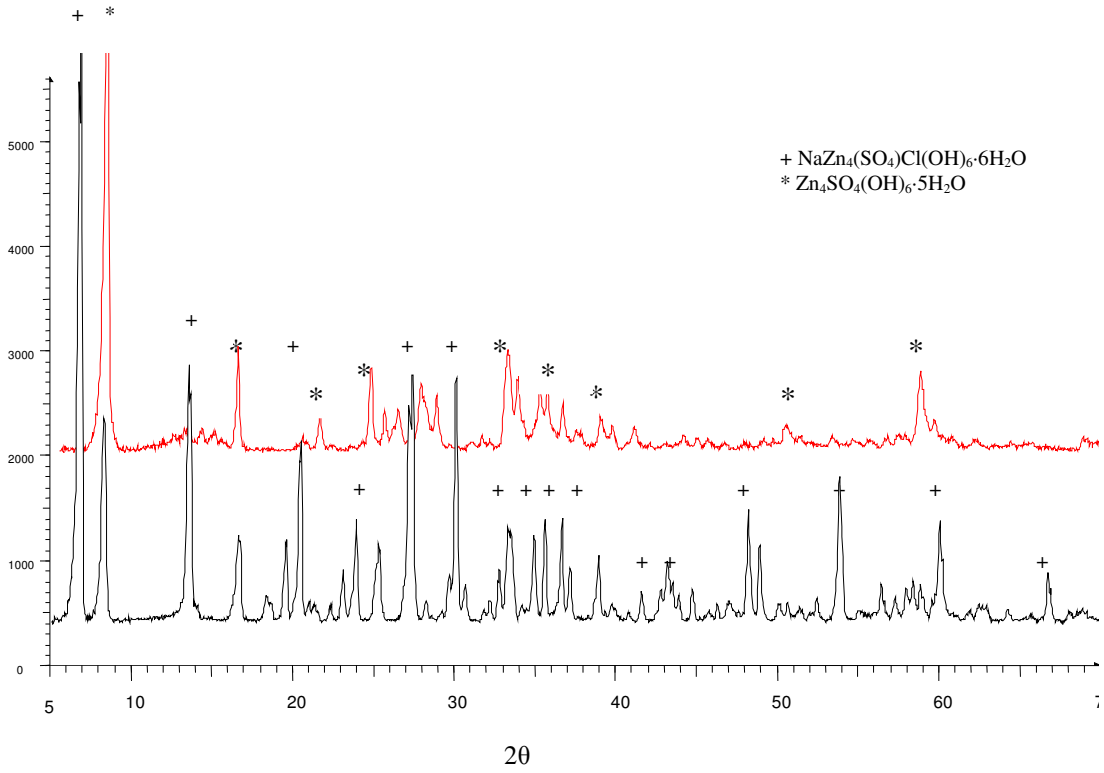

Figure 4.17 XRD patterns of $Zn_4SO_4(OH)_6{\cdot}5H_2O$ and $NaZn_4(SO_4)Cl(OH)_6{\cdot}6H_2O$

These phases can therefore form in the off-gas duct from ZnO, $ZnSO_4$, H_2O and NaCl. Hence the overall reactions can be written as:

$$ZnO + C/CO \leftrightarrow Zn + CO/CO_2$$

$$2SO_2 + O_2 \rightarrow 2SO_3$$

$$ZnO + SO_3 \rightarrow ZnSO_4$$

$$ZnSO_4 + 3ZnO + 8H_2O \rightarrow Zn_4SO_4(OH)_6{\cdot}5H_2O$$

$$ZnSO_4 + 3ZnO + NaCl + 9H_2O \rightarrow NaZn_4(SO_4)Cl(OH)_6{\cdot}6H_2O$$

Figure 4.19 schematically shows the dust formation mechanisms in semi-closed SAFs. It can be divided into four categories:

a. Vaporisation of elements or compounds from high temperature zones (1): Halite (NaCl) in the ferrochrome dust is a vaporisation product when the

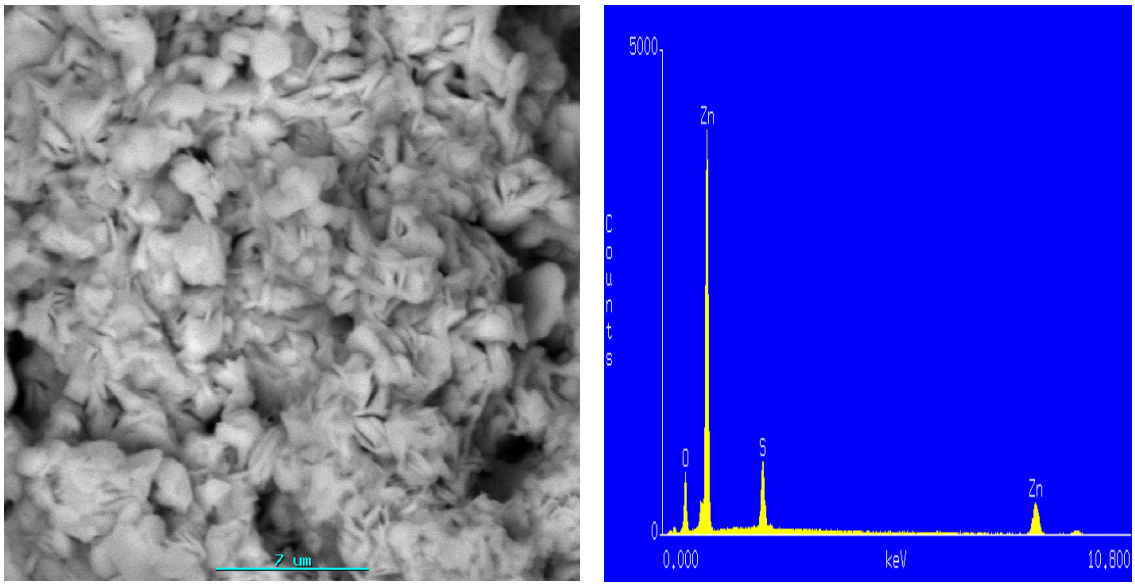

(a) $Zn_4SO_4(OH)_6{\cdot}5H_2O$

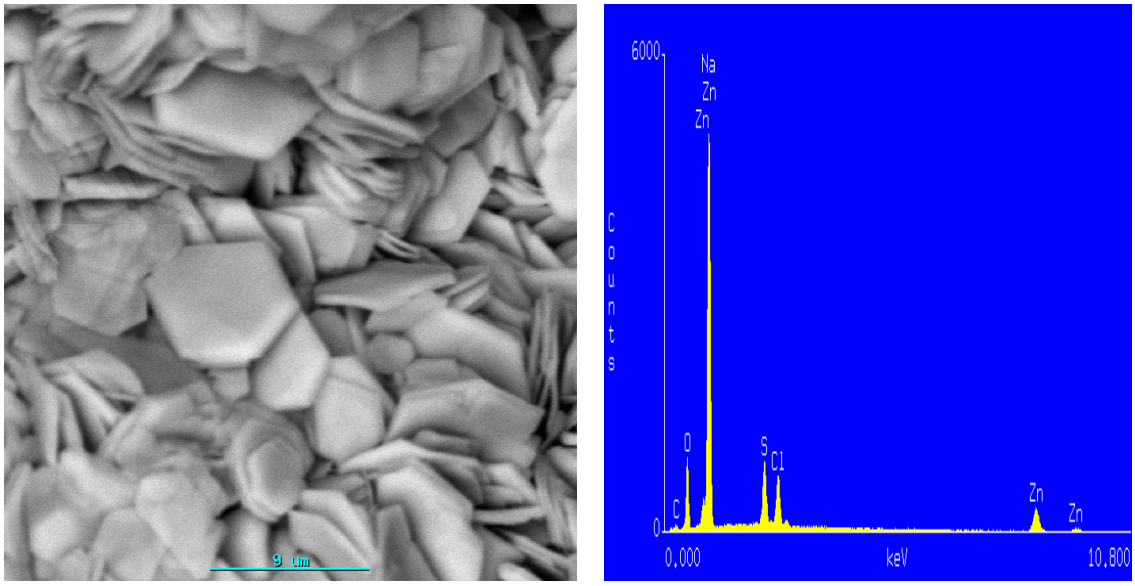

(b) $NaZn_4(SO_4)Cl(OH)_6{\cdot}6H_2O$

Figure 4.18 Secondary electron image and EDS spectrum of the synthetic crystals (a) $Zn_4SO_4(OH)_6{\cdot}5H_2O$ and (b) $NaZn_4(SO_4)Cl(OH)_6{\cdot}6H_2O$

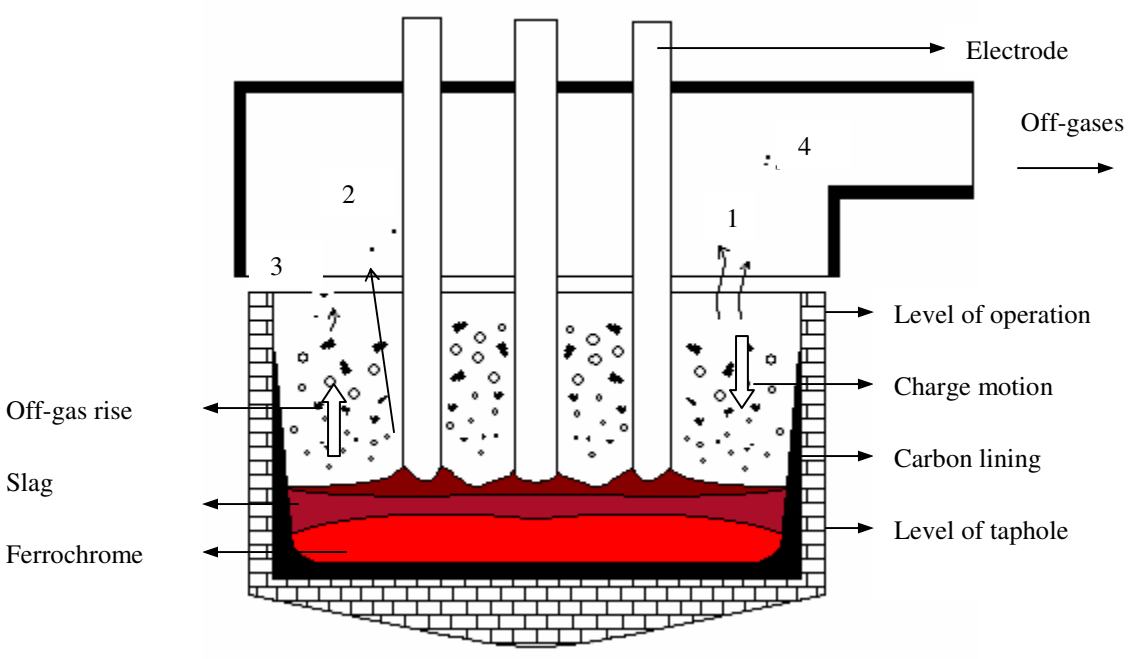

Figure 4.19 Dust formation mechanisms in semi-closed SAF

charge enters the high temperature zone of the SAF. Cristobalite (SiO_2), periclase (MgO) and ZnO are the oxidation products of oxide species that were fumed through a reduction reaction with carbon or carbon monoxide.

b. Ejection of slag and metal via the holes of the electrodes (2):
c. Charge materials that are directly captured in the off-gas (3):
   Carbon-bearing particles, quartz and chromite particles in angular shape present in the dust originate from the charge fines that were entrained in the off-gas.
d. Phases and reaction products that form in the off-gas duct from species in the off-gas (4):

The carbon-bearing particles, quartz and chromite particles present in the dusts originate from the charge fines, which were entrained in the off-gas. NaCl and ZnO are vaporisation products that formed during production. The metal and slag droplets were presumably ejected from the holes of the electrodes, while forsterite (Mg_2SiO_4) and the small amount of hydrate crystals [$Zn_4SO_4(OH)_6{\cdot}5H_2O$ and $NaZn_4(SO_4)Cl(OH)_6{\cdot}6H_2O$] formed in the off-gas duct via chemical reactions. Anorthite [$(Ca,Na)(Si,Al)O_8$] that is

present in the ferrochrome coarse dust, precipitated from the slag droplets during cooling in the off-gas duct.

4.3.3 The formation mechanisms of filter cake

The filter cake contains crystalline CaF_2, $CaSO_4$ and $CaCO_3$, as well as amorphous metal hydroxides. By considering the waste acid treatment process, it can be concluded that the crystalline phases (CaF_2 and $CaSO_4$) are generated in the neutralisation and reduction steps, $CaCO_3$ is the reaction product of the remnant lime particles with the carbon dioxide in the atmosphere, while the amorphous phases are generated in the precipitation step.

The overall reactions of the pickling acid treatment process can be summarised as follows:

Neutralisation step: $CaO + H_2O \longrightarrow Ca(OH)_2$ and $Ca^{2+} + SO_4^{2-} \longrightarrow CaSO_4$

$H^+ + OH^- \longrightarrow H_2O$ and $Ca^{2+} + 2\,F^- \longrightarrow CaF_2$

Reduction step: $3Fe^{2+} + Cr^{6+} \longrightarrow 3Fe^{3+} + Cr^{3+}$ and $Ca^{2+} + SO_4^{2-} \longrightarrow CaSO_4$

Precipitation step: $CaO + H_2O \longrightarrow Ca(OH)_2$ and $M^{n+} + n\,OH^- \longrightarrow M(OH)_n \downarrow$

(M represents metal cations such as Cr^{3+}, Fe^{3+} and Ni^{2+}).

4.3.4 Measures to reduce waste generation

Table 4.1 shows the process parameters that possibly influence dust formation during stainless steelmaking and ferrochrome production. Since ejection of slag or metal due to the bursting of the bubbles is the major dust formation mechanism in the stainless steel plant, measures should be taken to control the decarburisation reaction by changing the blowing (O_2 or Ar/O_2) time and rate as well as the position of the lance in the EF and converter. Slopping should also be minimised. To avoid vaporisation from the molten bath, the concentrations of volatile components in the scrap and molten ferrochrome should also be controlled. Moreover, the time of addition, method of addition (top charging or bottom injection), quantity and quality of charge materials influence the quantity of the dust particles that are directly captured in the off-gas.

Table 4.1 Parameters that possibly affect EF dust formation

Formation mechanisms	EAF smelting	AOD or CLU converter	Ferrochrome production
Vaporisation	Properties of charge (scrap and molten ferrochrome)	-	Raw materials properties
Directly captured during charging	The time of addition, type of addition (top charging or injection), quantity and quality of charge		Particle size distribution of charge
Ejection or bursting of bubbles	Oxygen blowing volume and time	Ar/O_2 ratio	Arc fluctuating
	Slag or non-slag operation	Blowing time, rate and temperature of gas mixture	Furnace type (open, semi-open or closed)

The output of ferrochrome fine dust is approximately 40 times by mass that of the ferrochrome coarse dust in a semi-closed SAF. It is therefore more important to reduce the formation of ferrochrome fine dusts than it is to reduce the amount of ferrochrome coarse dust. However, the volatile substances are the main components in the ferrochrome fine dusts. The volatile components (Na_2O + K_2O + ZnO + SO_3 + F + Cl + LOI) constitute up to ~ 44 wt % and ~ 30 wt% of FCD1 and 2, respectively (Table 3.2). Thus, controlling the quality of the raw materials, especially the volatile components in the coal, coke and charcoal, is a major task in reducing the amount of dust formed during ferrochrome production. Furthermore, small particles of raw materials should be avoided during charging in order to directly reduce the amount of dust that is carried off in the off-gas. It can be first agglomerated after which it is charged into the SAF.

Regarding the reduction of Cr (VI) formation during the production of ferrochrome: The temperature profiles, chemical compositions of the off gases and dusts, and the crystalline phases that are present in the dusts at different positions in the off gas duct, i.e., from the gas extraction hood to the bag house filters, need to be comprehensively investigated. The modelling of the behaviour of the off gas and dust in the duct is also very important. This can reduce the degree of Cr (VI) generation from the furnace to the bag house filter dust plant. A reduction in Cr (VI) generation in the furnace can be achieved by using

closed SAF operation, which will create more reducing conditions at the top of the furnace [145].

4.4 Conclusions

In the present chapter, the formation mechanisms of Cr(VI)-containing EF dust and filter cake were studied based on a microstructural investigation and FACTSage calculations. The following conclusions can be drawn:

1) Stainless steel dust contains particles that are irregular in shape, spherical or near spherical particles and particles coated with slag or oxides.
2) Stainless steel dust is formed by the entrainment of charge materials, evaporation or volatilisation of elements and ejection of slag and metal by spitting or the bursting of gas bubbles.
3) Ferrochrome fine dusts consist mainly of clusters which contain charge materials, slag droplets as well as very fine SiO_2-MgO-ZnO-$(Na,K)_2O$ based particles. The coarse particles consist of reductant, slag droplets and chromite particles.
4) Ferrochrome dusts are formed by the ejection of slag and metals droplets from the electrode hole, the entrainment of charge materials, vaporisation as well as the formation and precipitation of compounds from vaporised species in the off-gas duct.
5) Filter cake contains crystalline phases (CaF_2, $CaSO_4$ and $CaCO_3$) and metal rich amorphous phases. The crystalline phases (CaF_2 and $CaSO_4$) are generated in the neutralisation and reduction steps due to super saturation, while the metal rich amorphous phases are generated in the precipitation step.